Article

Site-Selective Surface-Enhanced Raman Detection of Proteins

Paolo Matteini, Maximilien Cottat, Francesco Tavanti, Elizaveta Panfilova, Mario Scuderi, Giuseppe Nicotra, Maria Cristina Menziani, Nikolai Khlebtsov, Marella de Angelis, and Roberto Pini

ACS Nano, **Just Accepted Manuscript** • DOI: 10.1021/acsnano.6b07523 • Publication Date (Web): 13 Dec 2016

Site-Selective Surface-Enhanced Raman Detection of Proteins

Paolo Matteini,[†] Maximilien Cottat,[†‡] Francesco Tavanti,[§‡] Elizaveta Panfilova,[#‡] Mario Scuderi,[$] Giuseppe Nicotra,[$] Maria Cristina Menziani,[§] Nikolai Khlebtsov,[#£] Marella de Angelis,[†] Roberto Pini[†]*

[†] Institute of Applied Physics "Nello Carrara", National Research Council, via Madonna del Piano 10, 50019 Sesto Fiorentino, Italy

[§] Department of Chemical and Geological Sciences, University of Modena e Reggio Emilia, via Campi 103, 41125 Modena, Italy

[#] Institute of Biochemistry and Physiology of Plants and Microorganisms, Russian Academy of Sciences, 13 Prospekt Entuziastov, 410049 Saratov, Russia

[$] Institute for Microelectronics and Microsystems, National Research Council, zona industriale strada VIII n.5, 95121 Catania, Italy

[£] Saratov National Research State University, 83 Ulitsa Astrakhanskaya, 410012 Saratov, Russia

KEYWORDS: SERS; biomolecules; plasmonic nanoparticles; silver nanocubes; crystal facets; computational simulations; phosphate buffer

ABSTRACT

Strategies for protein detection *via* surface-enhanced Raman spectroscopy (SERS) currently exploit the formation of randomly generated hot spots at the interfaces of metal colloidal nanoparticles, which are clustered together by intrusive chemical or physical processes in presence of the target biomolecule. We propose a different approach based on selective and quantitative gathering of protein molecules at regular hot spots generated on the corners of individual silver nanocubes in aqueous medium at physiological pH. Here, the protein while keeping its native configuration experiences an intense local E-field, which boosts SERS efficiency and detection sensitivity. Yet uncontrolled signal fluctuations caused by variable molecular adsorption to different particle areas or inside clustered nanoparticles are circumvented. Advanced electron microscopy analyses and computational simulations outline a strategy relying on a site-selective mechanism with superior Raman signal enhancement, which offers the perspective of highly controlled and reproducible routine SERS detection of proteins.

Surface enhanced Raman spectroscopy is a powerful tool for obtaining vibrational information from analytes that are present in low concentration in different chemical environments.[1,2] The electromagnetic fields localized at the surface of plasmonic nanostructures are responsible for enhancing the Raman signal of an adsorbed molecular target. This has tremendously expanded the potential of Raman spectroscopy inspiring a number of applications in the molecular detection and sensing fields.[3,4] In fact, the Raman scattering represents a minimal part of the light scattered by a molecule of interest, *i.e.* typical Raman cross sections are very small so that the analysis of many systems cannot be envisaged by conventional Raman. On the other hand, scattering efficiencies enhanced by several orders of magnitude (typically 4 - 8) provided by the excitation of the localized surface plasmon resonances (LSPRs) of silver or gold nanostructures can offer ultra sensitivity and detection of trace species. In some particular cases, atto-molar detection has been accomplished in SERS experiments on small aromatic molecules such as derivatized mercaptobenzenes or dyes like rhodamine 6G or crystal violet, which efficiently adsorb or display a strong chemical affinity for the metal surfaces.[5,6]

The possibility of SERS to operate a label-free detection providing the "fingerprint" of the molecule under study also in aqueous media, has become highly attractive for protein analysis.[7-10] In fact, the enhanced spectrum of a protein can give insight in its composition, conformation, function and protein-ligand interactions. However, despite substantial attempts have been made, the SERS detection of proteins has turned out demanding and still far from becoming an established analytical tool for real applications. Main concerns for a standardized SERS-based identification of proteins include sensitivity, reproducibility and conservation of the native state.[11-14] Current strategies for protein detection *via* SERS are based on chemically or physically aggregating noble metal colloids in the presence of the target protein. This popular approach

utilizes high field intensities produced at the interfaces between citrate-capped clustered nanoparticles, which are traditionally fabricated by the Lee & Maisel method.[15] However, the distribution of these highly localized positions of very high enhancement ("hot spots") is nonuniform inside the clustered nanoparticles,[16] which generates bright signals but confers scarce reproducibility and severe point-to-point variability.[9,17] Nonetheless, the LSPRs of aggregated colloids may dramatically vary as a function of the aggregation rate and time:[18,19] as a consequence, unless tuning in real time the illumination conditions (*i.e.* power density and acquisition time), photothermal and photodegradation processes can occur during the course of the SERS measurement, making Ag aggregates suffering from high photoinstability.[20] Lastly, the presence of a high charge density conferred by the capping agent as well as the chemical (addition of salts, pH change, *etc*.) or physical (heating, drying, *etc*.) methods used for eliciting particle aggregation may cause irreversible denaturation and loss of the native structure and functionalities of the protein.[21-23] Possible attempts to overcome the problems outlined above have been recently based on the use of bidimensionally-assembled SERS substrates. Here a regular hot spot array distribution confined in a planar layer as obtained by top down[24,25] or bottom up strategies[26,27] appears favorable in generating uniform SERS signals and superior reproducibility, without detrimental chemicals or invasive steps needed for the analysis. A more recent proposal suggested the convenience of conducting SERS measurements with nanoparticles that are aggregated within the focal laser spot by repulsive scattering forces to getting control over the aggregate size.[28]

In this work we demonstrate the feasibility of a SERS detection of proteins in aqueous medium at physiological pH, relying on a site-selective detection at the hot spots of individual nanoparticles in turn assuring high reproducibility and sensitivity. This is accomplished by

exploiting the synergic role of the SERS substrate, *i.e.* silver nanocubes, providing intensified electromagnetic field concentrated on their corners, and the capping agent, *i.e.* polyvinylpirrolidone (PVP), which confers elevated colloidal stability in the presence of the biomolecule and regional passivation of the cube faces.

RESULTS AND DISCUSSION

An electron microcopy characterization of silver nanocubes is visualized in **Figure 1** while additional details concerning the size distribution within our particle batches and particle surface charge are reported in Supporting Information (**Figures S1-S3**). Nanocubes of ~50 nm size (**Figure 1a**) were obtained by the sulfide-mediated polyol method in which Ag(1) is reduced to Ag(0) by ethylene glycol in the presence of PVP and a trace amount of Na_2S.[29,30] The supersaturation of as-formed Ag atoms triggers their assembly to form seeds that then grow into the final Ag nanocubes. PVP is here used as a structure-directing polymer with high affinity toward the {100} facets of the initial Ag nanoseeds, which drives a selective reduction of silver atoms on their free {111} facets thus resulting in an anisotropic growth of the nanoparticle in the form of cube. Indeed previous studies have demonstrated a 10^9 times stronger preference of PVP in binding to the {100} facets with respect to the {111} Ag facets.[31] Concurrently, a highly dense surface coverage of PVP is expected on the final nanocubes, which are primarily enclosed by six {100} facets (**Figures 1b,1c**).[32] However ~50 nm-size silver nanocubes, as obtained by using PVP as capping agent, typically show slightly truncated or rounded corners,[32] which originate from an uncompleted growth of the {100} seed facets, this effect being alleviated at larger cube sizes. As a matter of fact the aberration-corrected scanning transmission electron microscopy (ac-STEM) analysis of our nanocubes shows corners with a 6-7 nm radius of curvature and a

stepped surface composed of a mixture of {110} and higher Miller index facets (**Figure 1d**). Additionally, while a PVP layer of 1.1 – 1.8 nm thickness is observed on the cube sides as expected on the basis of favorable {100} facets/PVP interactions,[32] it becomes sparse and extremely thin on the corners as bright field transmission electron microscopy (TEM) micrographs of **Figures 1e and 1f** indicate. The thickness of a monolayer of PVP repeating units is estimated to be 0.3 - 0.5 nm,[32] thus we can conclude that PVP is arranged as a multiple layer on the cube faces and as an incomplete and patchy monolayer at the corners.

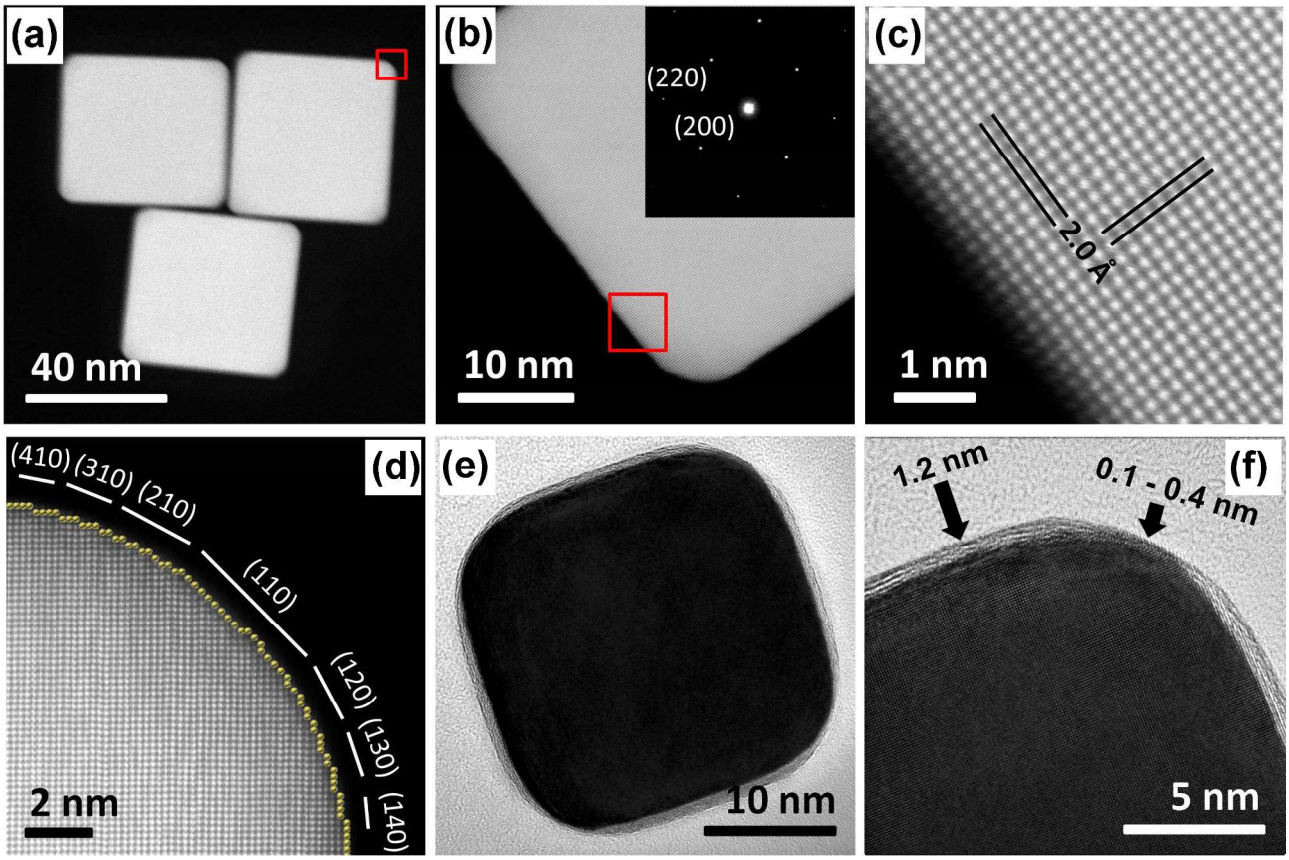

Figure 1. (a) annular dark-field (ADF) STEM image of a cluster of three nanocubes. (b) ADF STEM image of a nanocube and corresponding selected area electron diffraction pattern (inset) showing spots of {200} reflections. Both image and inset indicate that the nanoparticle is a piece of a single crystal with faces oriented along [100] equivalent directions. (c) High resolution ADF

STEM image of a nanocube portion (red square of (b)) showing a crystal lattice spacing of 2.0 Å aligned with the nanocube border. The evidenced lattice can be indexed to the {200} reflection of face-centered cubic (fcc) Ag. (d) High resolution ADF STEM image of a nanocube corner (red square of (a)) showing its microfaceting composition. (e, f) Bright-field TEM images of a single nanocube showing the amorphous PVP layer. In (f) the reduced thickness of the PVP layer on the corner is evidenced.

We note that the choice of silver nanocubes has been revealed as largely preferable in fundamental SERS studies because of their well-established superior SERS efficiency with respect to spherical or quasi-spherical nanoparticles,[33] albeit a more extensive use of the latter in experiments dealing with SERS and biomolecules. SERS enhancement factor can be as low as 10 - 10^3 for non-optimized SERS assays involving spherical nanoparticles but can grow of about two-three orders of magnitude when nanoparticles containing sharp features are concerned.[33] This is corroborated by a theoretical simulation of the E-field distribution on 50 nm-size silver nanocubes placed in an aqueous environment as displayed in **Figure 2a-c**. In a nanocube surface electrons strongly accumulate on the corners of the nanoparticle producing a highly confined E-field (**Figure 2a**), which largely influences the SERS activity of the particle. We estimated the maximal local field at the corners to be $\left|E/E_0\right|_{\max} \sim 22$, which is three times higher than the average field on the faces $\langle\left|E/E_0\right|\rangle_{faces} \sim 6$. Thus, as SERS enhancement is proportional to the fourth power of the E-field, the corner sites should contribute ~10^2 times to the maximum SERS enhancement as compared to the cube faces. In **Figure 2b** the enhancement factor (EF) variation along the profile between the center of a cube face and a cube corner is displayed. An EF_{MAX} of

2×10^5 is obtained, which is well in accordance with previous literature.[34,35] In general the EF values on the corners largely prevail over the total EF (**Figure 2c**).

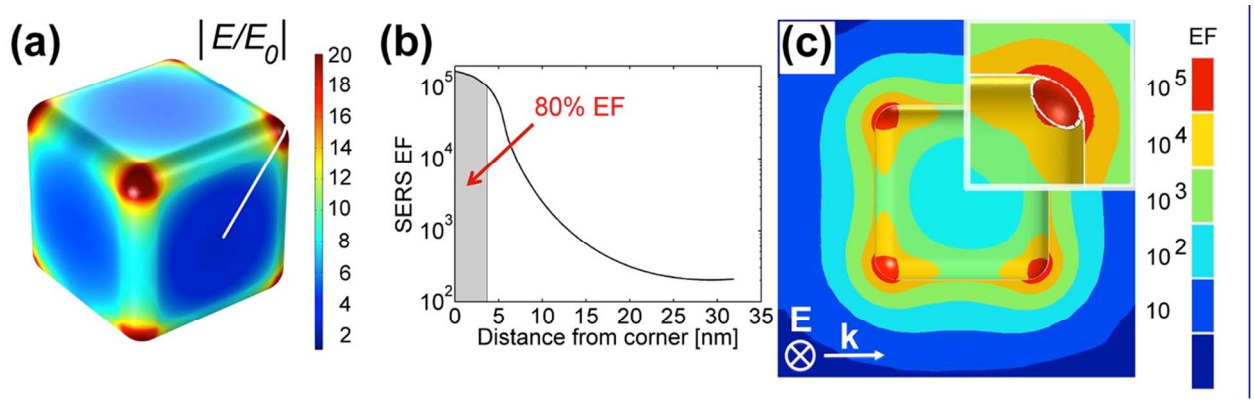

Figure 2. (a) FEM simulation of the distribution of the E-field over the surface of a 50 nm-size nanocube; (b) Profile of the EF distribution along the white line shown in (a) connecting the apex of a corner to the center of a face. The corner site (approximated as a calotte-shaped section as defined in **Figure S4** and outlined in (c)) provides 80% of the total SERS signal (gray band in the graph); (c) Side view of the spatial EF distribution over a cube as expressed in logarithmic scale: the EF scales by an order of magnitude by passing from a colored zone to a contiguous one. Inset: magnified view of the corner; the dashed line defines a 68°-subtended calotte resembling the PVP-free area as estimated from TEM analysis (see **Figure 1f and Figure S4**).

In a typical SERS experiment a 5 µL aliquot of nanoparticle solution is suspended onto a 3 mm^2-rounded hole that was obtained from a cap-shaped polypropylene support (1 cm height × 2 cm diameter). By this configuration down to pico-/femto-moles of analyte can be processed per measurement while accurate laser focusing control and extensive investigation of the sample are assured (**Figure 3a**).

In this study we focused on cytochrome c (cytC) because it represents a model protein characterized during several Raman and resonant-SERS studies.[18,36-40] CytC is a hemoprotein and part of the electron transport chain of mitochondrial respiration. Its heme is bound to the protein through the porphyrin substituents by two cysteine side chains, while methionine-80 and histidine-18 act as axial ligands of the central iron (**Figure 3b**). A nice matching between the plasmon resonances of Ag spherical nanoparticles and the resonant excitation of the Soret absorption band (410 nm) or of the Q band (from 500 to 550 nm) of the heme group of cytC (**Figure S3**) has been previously exploited to produce effective SERS spectra of the protein.[18,40,41] This configuration appears strategic to gain insights into the chemical and structural characteristics of the heme group after protein adsorption. The main LSPR of silver nanocubes is peaked at 455 nm showing a tail extended toward the yellow-red region (**Figure S3**), offering further SERS capability at longer excitation wavelengths, which is of interest for testing also non-resonant SERS effects.

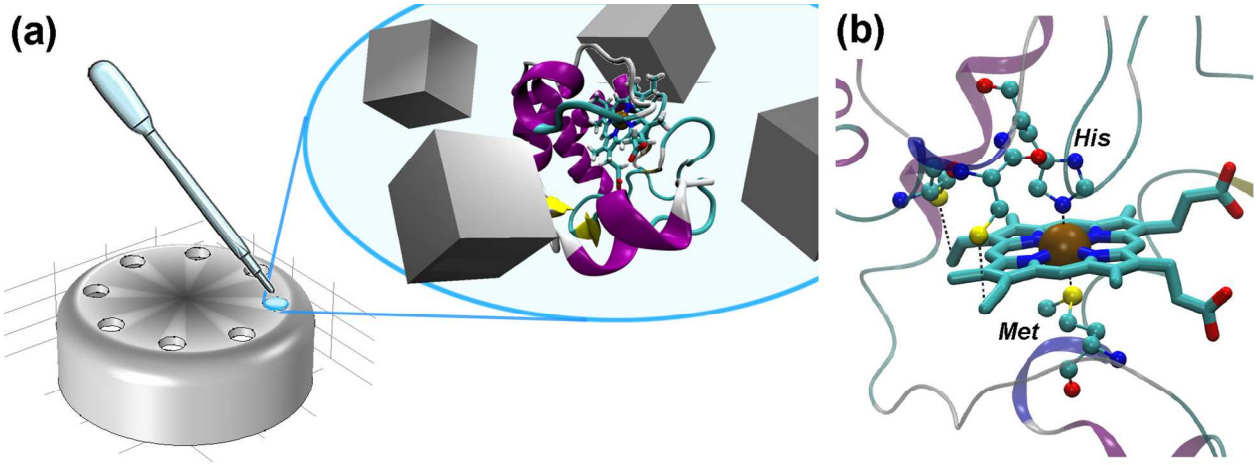

Figure 3. (a) Sketch of the method used for deposition of Ag nanocubes/protein mixtures. Single 5 μL aliquots are dropped into 3 mm^2-rounded holes obtained from a polypropylene support. A total of 8 holes have been produced along the perimeter of the cap to provide extended capability for multiple measurements. Once suspended the solution exposes a smooth

~3 mm^2 surface parallel to the Raman detection system offering a long lasting focal plane, which instead rapidly changes when the solution is dropped onto a solid substrate.[42] Approximately a 10 minutes period is available before observing a minimal change in the laser focus and a 60 minutes period before complete evaporation of the solution at room temperature, which appear long enough for an extensive investigation of the sample. (b) Heme group of cytC containing a central iron ion that is connected to the protein by two covalent heme-cysteine thioether linkages and is axially coordinated by a histidine and a methionine residues. The heme group is located near the exterior of the protein with its hydrocarbon side chains interior and its polar propionate chains exterior.

Figure 4 presents a comparison between the SERS signal and the Raman signal of a 1×10^{-8} M and a 1×10^{-3} M cytC solutions, respectively, once analyzed with a 532 nm laser excitation. A collection of the detected frequencies with peak assignment[37,39,40,43-45] is reported in **Table 1**. We anticipate that the plasmon resonances of nanocubes after protein incubation resemble those of individual cubes as measured in phosphate buffered solution (**Figure S5**). Thus we can infer that the SERS samples consist of isolated nanocubes, which are stabilized by the PVP coating. Due to resonance condition, Raman and SERS signals are dominated by the heme vibration modes ν_{15} (B_{1g}) 748 cm^{-1}, ν_{22} (A_{2g}) 1126 cm^{-1}, ν_{30} (B_{2g}) 1168 cm^{-1}, ν_{21} (A_{2g}) 1315 cm^{-1}, ν_4 (A_{1g}) 1373 cm^{-1}, ν_{20} (A_{2g}) 1401 cm^{-1}, ν_{19} (A_{2g}) 1584 cm^{-1} and ν_{10} (B_{1g}) 1634 cm^{-1}. The position of the oxidation state marker band ν_4 is in line with an oxidized form of the protein, which is preserved after its adsorption on the nanocube surface.[38] At first reading, the high similarity between the intensity pattern of the SERS and Raman spectra discards the occurrence of relevant changes in the secondary or tertiary structure of cytC.

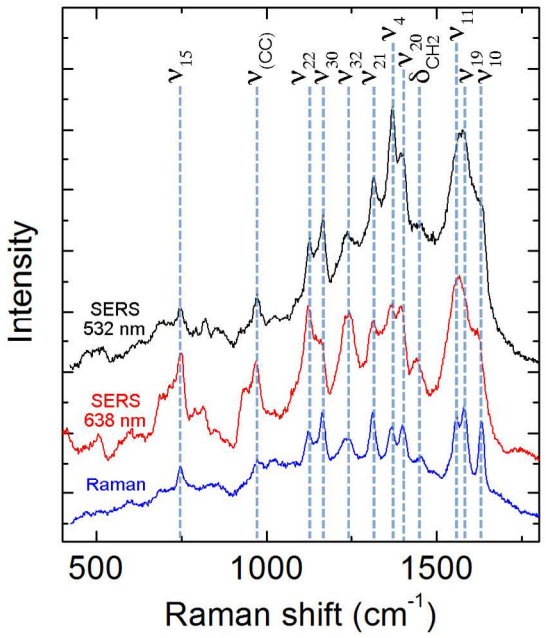

Figure 4. SERS spectra of cytC/silver nanocubes mixtures obtained by using 532 nm (black) and 638 nm (red) excitation wavelengths. The concentration of cytC is 1 $\times 10^{-8}$ M. The Raman signal of a 1 $\times 10^{-3}$ M cytC solution is also reported for comparison (blue). Integration time (10 s) and laser power at the sample are 4.8 mW at 532 nm and 2.1 mW at 638 nm. Same experimental parameters are used for the SERS and Raman measurements at λ_{ex} = 532 nm so that relative spectra are directly comparable. The spectra are offset for clarity and represent the average over 50 measurements from three replicated samples.

Table 1. Peaks assignment for Raman and SERS signal of cytC (n.r. = not resolved)

Raman	SERS			
λ = 532 nm	λ = 532 nm	λ = 638 nm	Mode LS	Mode HS
n.r.	n.r.	686	ν_{CS}	
748	748	748	ν_{15} (B_{1g})	
		825, 855	Tyr Fermi doublet ?	
	n.r.	930	ν_{46} (E_u)	
974	974	973	ν_{CC} propionate	
	n.r.	1083	δ_{CH3}	
1126	1126	1126	ν_{22} (A_{2g})	
1168	1168	1168	ν_{30} (B_{2g})	
n.r.	n.r.	1232	ν_{13} (B_{1g})	
n.r.	n.r.	1247	δ_{CH2} twist propionate	

1315	1315	1315	$\nu_{\square\square}$ (A_{2g})	
1373	1373	1373	ν_4 (A_{1g})	
1401	1401	1401	ν_{20} (A_{2g})	
n.r.	n.r.	1453	δ_{CH2} wag propionate	
	1492	n.r.		ν_3 (A_{1g})
1500			ν_3 (A_{1g})	
1557	n.r.	n.r.	ν_{11} (B_{1g})	
	1570	n.r.		ν_{19} (A_{2g})
1584	1584	n.r.	ν_{19} (A_{2g})	
	n.r.	1610	Trp, Tyr, Phe ?	
	n.r.	1620		ν_{10} (B_{1g})
1634	1634	n.r.	ν_{10} (B_{1g})	

Most of the mode assignments of the SERS spectrum of cytC with the 638 nm laser excitation (**Figure 4, Table 1**) are the same as those from the green excitation. However, additional peaks from the heme group become now resolved at 1247 cm^{-1} and 1453 cm^{-1}, which are associated with the twisting and wagging vibrations of the propionate CH_2 groups.[44] Other additional bands can be tentatively ascribed to amino acid residues such as the 686 cm^{-1}, the 1083 cm^{-1} and the 1610 cm^{-1} peaks, which were previously assigned to ν_{CS} of Cys residues covalently binding the porphyrin moieties of the heme, δ_{CH3} and the ring stretching of Tyr, Trp or Phe, respectively.[46,47] The peaks at 825 cm^{-1} and 855 cm^{-1} may originate from the Fermi resonances of Tyr.[44,47] The presence of low-frequency components of the $\nu_{10,}$ ν_{19} and ν_3 modes at 1620 cm^{-1}, 1570 cm^{-1} and 1492 cm^{-1} in the SERS spectra of **Figures 4**, which do not appear in the Raman spectrum makes infer a direct protein-metal interaction. These bands are ascribed to a partial conversion from the low-spin to the high spin state of the protein,[38,43,48] which has been thoroughly investigated in previous studies and verified as a distinctive signal of surface adsorption without affecting the biological function.[38] Thus, clear evidence appears of a metal-protein interaction, which on the basis of the TEM micrographs of **Figures 1e,f** should be favored when the protein is physically

adsorbed on the cube's corners, while the access to the faces is chemically blocked because of the presence of a thick PVP layer.

Molecular dynamics (MD) simulations proved a useful tool to validate the above hypothesis, enabling the study of protein/nanocube interactions at atomic details. In particular, we performed MD simulations in water to inspect: 1) possible protein changes after its adsorption to the naked nanoparticle surfaces and 2) the affinity of cytC against silver surfaces in the presence of a PVP coating. First, a characterization of the interactions with silver {110} and {120} facets, which are mainly found at the corner sites (**Figure 1d**), was carried out. **Figure 5a** displays the calculated surface adsorption of the protein on the {110} facet: here the aminoacid residues that more frequently generate temporary interactions with the metal are highlighted and further listed in **Table S1**.

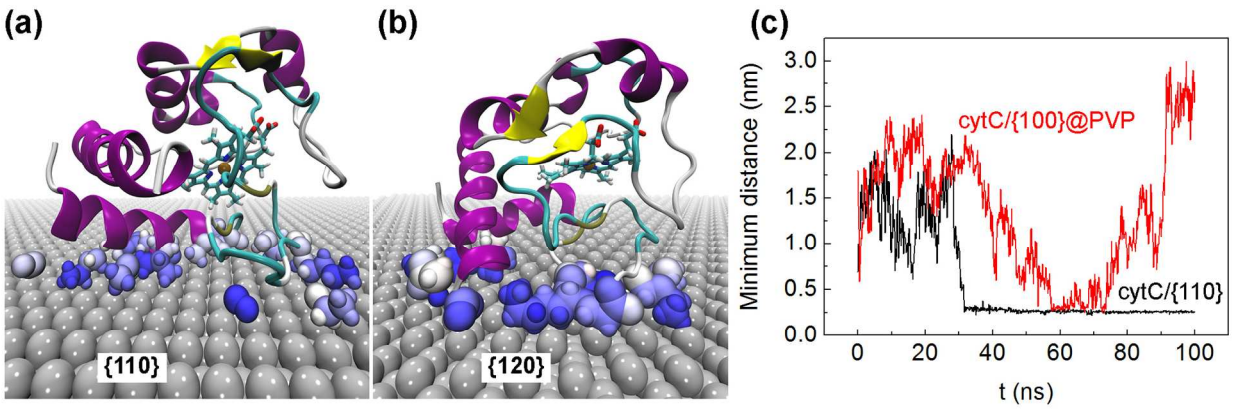

Figure 5. In (a) and (b) a representation of the contacts between cytC and the {110} and {120} silver surfaces, respectively, is visualized. Atoms in contact with the surface are colored from blue to white as a function of their contact persistence (blue = longer; white = shorter). Proteins are rendered in accordance with their secondary structures. In (c) the minimum distance between the protein and a {110} surface (black) and between the protein and a PVP-coated {100} surface, (red) during a 100 ns-long simulation time is reported.

Among others, favorable interactions between protein and silver can be provided by the side chain ε-amino group of Lys residues, as previously pointed out at bare gold interfaces.[49] Conversely, the possibility of heme degradation *via* thioether bonds breaking with irreversible modifications and protein denaturation[50,51] can be ruled out since no direct bonding of Cys-17 and Cys-14 is observed. The absence of aromatic aminoacid directly interacting with the metal is well in accordance with a scarce contribution of these residues to the SERS spectrum. However, the Tyr-97 assignment in the SERS spectra (**Figure 4a**) is supported by its reduced distance (~2.2 nm) from the metal found in the MD simulations (**Figure S6**). The proximity of the heme group to the silver surface (Fe^{3+}-surface distance = 1.2 nm) favors preferential SERS enhancement of the heme-associated moieties.[44] As a matter of fact, propionate modes as well as modes associated to heme-cysteine thioether linkages (**Table 1**) are more largely enhanced in SERS compared with Raman spectra (**Figure 4a**). Similar considerations can be applied to the adsorption configuration with the {120} facet (**Figure 5b**). Here the heme to surface distance is increased to 2 nm. The SERS signal intensity at this distance is predicted to drop by less than a 10 factor[39] relative to the heme distance from the {110} facet. Overall the MD simulations indicate that the adsorption of cytC on the bare silver surface almost unalters the native protein arrangement with negligible changes to the heme pocket laying at a safe distance from the metal and discarding the occurrence of irreversible modifications (**Figure S7**) in line with SERS outcomes.

A second aim of MD calculations consisted in evaluating the possibility of a reduced adsorption and retention effect of cytC on silver surfaces protected by a PVP layer. Computing the distance between cytC and the silver surface over a 100 ns-long simulation time, we found

that the protein is rapidly adsorbed onto the naked metal where remains irreversibly attached (**Figure 5c**). When the metal is protected by PVP, the protein transiently interacts with the polymer but the interaction strength is not enough to maintain the protein firmly adhered in turn resulting in a rapid desorption (**Figures 5c)**. We point out that a low affinity of proteins toward PVP-functionalized gold and silver nanoparticles has been previously stressed and ascribed to a passivation effect of the PVP coating preventing direct protein interactions with the nanoparticle surface.[52,53]

Taking advantage of the results of SERS and of MD we repeated the TEM analysis on nanocubes once incubated with the protein solution (**Figure 6**). Remarkably, the corners now appear covered by new material that sometimes is observed exceeding the thickness of the PVP adlayer on the rest of the particle. Thus the ensemble of evidences discussed above provides substantial endorsement toward a site-selective protein adsorption and a selective SERS detection on cube's hot spots.

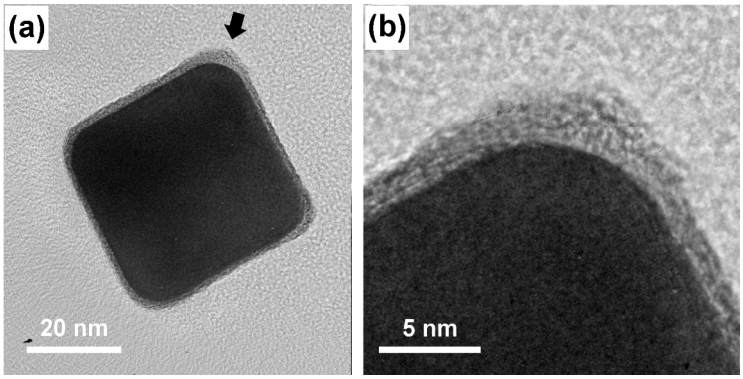

Figure 6. (a) Bright-field TEM image of a silver nanocube after incubation with 1×10^{-8} M cytC. A magnification of the corner is visualized in (b).

Previous reports dealt with the possibility of chemically discriminating different nanoparticle regions: *e.g.* a selective protection of different locations of gold nanorods and prisms with

functional molecules was reported.[54,55] In the framework of SERS, a site-selective detection of proteins on cube corners proves appealing for two main reasons: 1) SERS efficiency and in turn sensitivity can be enhanced upon concentrating the protein molecules exactly on the hot spots of the SERS system and 2) uncontrolled signal fluctuation consequent to a variable molecular adsorption to different particle areas can be avoided. That is, from one side every single protein molecule that is present in solution can be detected until the PVP-free surface on the cube tip is available: thus quantitative studies at low concentrations of protein can be performed. Another aspect concerns the reproducibility of the SERS analysis. Cube corners represent ~2.4% of the total particle surface (**Figure 2a**) showing a more homogeneous E-field distribution with respect to cube faces. Precisely, less than one order of magnitude in EF variability is simulated at each corner sites against more than three orders of magnitude of variability when moving from the center to the periphery of a face (**Figure 2c**). In general, by limiting the SERS analysis to confined regions showing uniform optical and chemical features appears advantageous for reliable SERS detection of complex analytes with low Raman cross sections such as proteins.

We evaluated the signal amplification provided by our SERS substrate with respect to normal Raman spectroscopy by calculating the SERS gain G (also called analytical enhancement factor) as well as the SERS enhancement factor EF.[28,56-58] While G is a rough estimate of the overall signal gain that can be offered by a SERS-active substrate, EF is a measure of the signal amplification experienced by each molecule on the nanostructure and requires an assumption of the number of molecules adsorbed on the nanoparticle's surface.

G can be defined as:

$$G = \frac{I_{SERS} / c_{SERS}}{I_{Raman} / c_{Raman}}, \qquad (1)$$

where I_{Raman} and I_{SERS} are the Raman and SERS signal intensities, c_{Raman} and c_{SERS} are the concentration values of the analyte solution used for the Raman and SERS measurements, respectively.

Instead, EF is defined as the ratio between I_{Raman} and I_{SERS} normalized to the number of probed molecules, *i.e.* the average number of molecules dispersed in solution N_{Raman}, for the Raman measurement, or adsorbed onto the nanocubes N_{SERS}, for the SERS measurement, which are present in the scattering volume (*i.e.* the laser spot):

$$EF = \frac{I_{SERS} / N_{SERS}}{I_{Raman} / N_{Raman}} . \qquad (2)$$

Both Eq. 1 and 2 require that Raman and SERS measurements are performed under identical experimental conditions, including laser wavelength, laser power, accumulation time, microscope objective, spectrometer, *etc*..

By comparing the 1373 cm^{-1} band intensity in the SERS spectrum at λ_{ex} = 532 nm of a 10^{-8} M cytC solution with the analogue in the Raman spectrum of a 10^{-3} M solution, a G ~10^5 value is obtained.

In the case of EF an estimate of N_{SERS} and N_{Raman} is required. Given that the volume probed by the laser spot remains the same for Raman and SERS measurements, N_{Raman} can be simply achieved by multiplying the concentration to the Avogadro number:

$$N_{Raman} = N_A c_{Raman} \qquad (3)$$

thus giving $N_{Raman} = 6 \times 10^{17}$ mL^{-1}. N_{SERS} can be calculated as the product between the number of molecules adsorbed on each nanocube (N_{mol}) and the number of nanocubes in the same volume considered for the calculation of N_{Raman} (*i.e.* N_{nano}):

$$N_{SERS} = N_{mol} N_{nano} \quad (4)$$

Precisely, we can estimate that a total of ~3300 cytC molecules can find accommodation on each cube, while ~80 molecules are sufficient to completely cover the cube corners (corresponding to ~10 molecules per corner, see Supporting Information for calculations). However, we may note that the molecules localized on the corners, *i.e.* $N_{mol} \simeq 80$, are largely those contributing to the SERS signal. In fact a total of 80% EF produced on the surface of a single particle is imparted by the hot spots localized on the corners as predicted in **Figure 2b**. Thus N_{SERS} can be estimated as 5×10^{12} mL^{-1} (being $N_{nano} = 6 \times 10^{10}$ mL^{-1} and N_{mol} taken as 80). With the above premise, an EF value of ~10^5 is obtained, which well matches the EF value averaged over a 3 nm-thick shell sector surrounding the corner (*i.e.* 1.6 × 10^5, **Figure 2c**), approximating the region occupied by the adsorbed protein. In our case the comparison between EF and G is of particular significance. In fact, similar G and EF values can substantiate that all the protein molecules that are dissolved in solution contribute to a similar extent to the final SERS signal. This condition is only justified by assuming that the molecules available in solution (*i.e.* ~100/cube at 1 × 10^{-8} M) are selectively adsorbed on the SERS hot spots *i.e.* on the cube

corners. Thus the extensive matching between G and EF values furnishes supplementary evidence of a confinement of protein molecules at the hot spots.[59]

Once established the main prerequisites to operating in a site-selective SERS configuration, we assessed the chance to perform quantitative, sensitive and reproducible SERS measurements. First, we registered the SERS response of different cytC solutions in a concentration range of physiological interest, by keeping unaltered the nanoparticle number. In particular the SERS spectra of 1×10^{-7}, 1×10^{-8} M, 6×10^{-9} M and 2×10^{-9} M at λ_{ex} = 532 nm and 638 nm are shown in **Figures 7a,b**. The SERS profile of the protein is regularly reproduced down to the last protein dilution, suggesting a limit of detection (LOD) of about 5 ÷ 10 nM at both excitation wavelengths. Thus a high sensitivity is apparent, which overcomes previous results involving the use of aggregated nanoparticles.[60-62] On the basis of proposed protocol, the 1×10^{-8} M cytC solution, corresponding to ~100 molecules per cube, should approximately resemble the saturation of protein molecules on the available space of the hot spots. Thus, while at lower concentration values a quantitative decrease in SERS signal can be observed, higher values actually appear ineffective in altering the intensity because the SERS signal is dominated by contributions from the adsorbed first protein monolayer.[18,63] Future assessments involving systematic adjustments of the molecules to nanoparticle ratio will shed light on the possibility of a quantitative analysis centered at higher and lower concentration values.

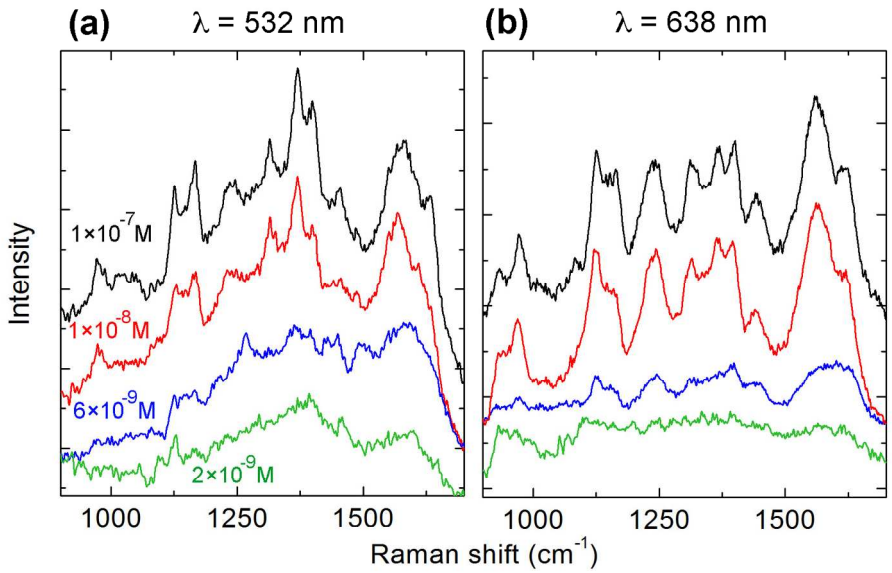

Figure 7. SERS spectra of cytC at concentrations of 1×10^{-7} M (black), 1×10^{-8} M (red), 6×10^{-9} M (blue) and 2×10^{-9} M (green) taken at λ_{ex} = 532 nm (left) and λ_{ex} = 638 nm (right). Integration time (10 s) and laser power at the sample are 4.8 mW at 532 nm and 2.1 mW at 638 nm. The spectra are offset for clarity and represent the average over 10 measures from a single sample.

Another fundamental aspect in the practical applications of SERS is the collection of uniform signals, which is associated with a regular distribution of hot spots. The site-selective adsorption on the hot spots of the nanocubes proves an effective strategy for minimizing signal fluctuations. In fact, once adsorbed on the cube corners, protein molecules are exposed to a homogeneous amplification in their Raman signal. Besides, working with isolated nanoparticles further improves signal stability, as we actually verified according to **Figure 8**. Typically we observed a maximal relative standard deviation (RSD)[57] not exceeding 10% for the main Raman peaks of cytC at both λ_{ex} = 532 nm and 638 nm, which resembles RSD values ascribed to SERS substrate with high spatial uniformity and reproducibility.[64]

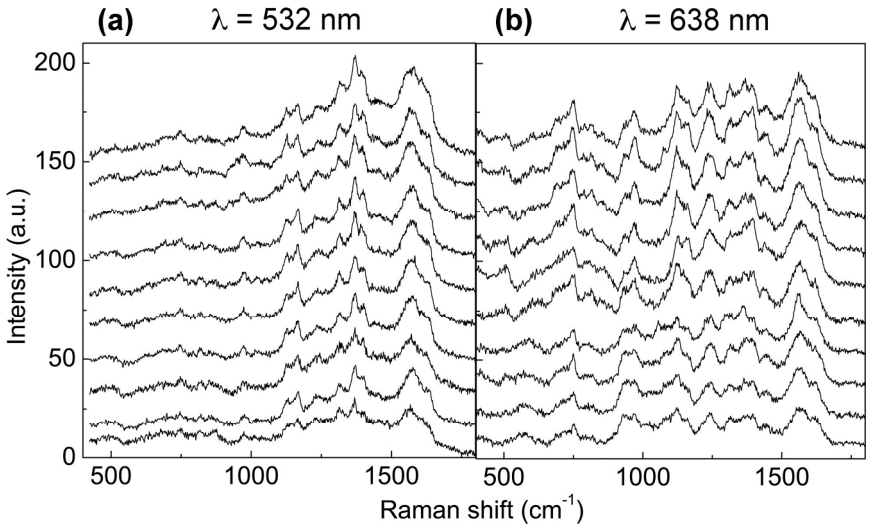

Figure 8. Series of random SERS spectra from three Ag nanocube dispersions incubated with 1 × 10^{-8} cytC at λ_{ex} = 532 nm (a) and at λ_{ex} = 638 nm (b). RSD values of the intensity referred to the 1373 cm^{-1} peak are 9% at λ_{ex} = 532 nm and 10% at λ_{ex} = 638 nm.

CONCLUSIONS

In conclusion, we have revealed a strategy to generate intense, sensitive and stable SERS spectra from proteins in liquid at physiological pH and at low concentration, by exploiting the optical and chemical properties of nanocubes. In our scheme a PVP coating shields the contacts between protein and metal at the cube faces and drives the preferential interaction of the protein with the corners, where PVP is rare. In this way the protein molecules gather on the hot spots of the SERS system where they experience an intense E-field. Accordingly, undesirable signal fluctuations caused by molecular adsorption to different particle areas are circumvented. The use of PVP also assures an optimal colloidal stability during the incubation phase with the protein in physiological buffer as well as during the course of the measurement, discarding the occurrence of aggregation events. The scheme here adopted yields high sensitivity and reproducibility in

both resonant and nonresonant excitation conditions of the protein and offers the perspective of highly controlled and reliable routine detection of proteins based on SERS.

EXPERIMENTAL SECTION

Materials

Cyt C from bovine heart and all salt reagents were purchased from Sigma Aldrich and used as received. A stock solution of protein at 1×10^{-4} M was prepared by dissolving the protein in a 7 mM phosphate buffer solution (pH 7.4). Phosphate buffer was prepared by mixing proper amounts of Na_2HPO_4 and NaH_2PO_4 in ultrapure Milli-Q water. Cyt C samples in the 1×10^{-5} M to 1×10^{-7} M range were prepared immediately before the incubation with the cubes by diluting with buffer.

Silver nanocube preparation

Ag nanocubes were prepared through a protocol reported by Skrabalak *et al.*[29] with minor modifications.[30] In brief, 30 mL of ethylene glycol was added to a 250-mL round-bottomed flask and was heated in an oil bath at 150 °C under magnetic stirring. After 50-min preheating, a flow of argon was introduced at a rate of 1200 mL/min. Ten min after, 0.35 mL of 3 mM sodium sulfide solution in ethylene glycol (EG), was quickly injected into the preheated EG solution, followed by injection of a PVP (MW = 55000 Da) solution in EG (7.5 mL, 20 g/L) and 8 min later by injection of a silver nitrate solution in EG (2.5 mL, 48 g/L). Shortly after the addition of $AgNO_3$, the reaction solution went through four distinct stages of color change from golden yellow to deep red, reddish gray, and then green ocher. The reaction was controlled by approaching of major absorption peak to 450 nm. Then, the reaction was stopped by addition of

ice-cooled acetone and placing the reaction flask in an ice-water bath. The resultant product was washed by centrifugation (12000 g, 30 min) and redispersed in acetone, followed by centrifugation (12000 g, 30 min) and redispersion in ethanol to remove excess of EG and PVP. Finally, the Ag nanocubes were redispersed in 20 mL of ethanol. The suspensions of cubes thus obtained were stored in centrifuge tubes at -20°C and used within 3 months from their fabrication.

Surface-enhanced Raman scattering spectroscopy

Prior to incubation, 10 µl of nanoparticles were diluted in phosphate buffer and sonicated to avoid aggregation. Then 5 µL of protein sample were mixed with the nanocubes to obtain a final volume of 500 µL and final protein concentrations in the 10^{-7} M ÷ 10^{-9} M range. Incubation time was of two hours at room temperature, then samples were concentrated to 30 µL after centrifugation, obtaining a final particle density of 1×10^{12} particles/mL. SERS experiments were carried out using a micro-Horiba Xplora system coupled to 532 nm and 638 nm lasers. The back-scattering light was collected by a 10× microscope objective with 0.25 NA, which generates a ~7 µm-large laser beam waist and provides an average SERS response minimizing possible local signal variability. Acquisition time of each spectrum was 10 s with 2 accumulations. Laser powers at the sample of 4.8 mW at 532 nm and 2.1 mW at 638 nm were measured. Diffraction gratings of 1800 g/mm and 1200 g/mm were used at 532 nm and 638 nm, respectively. SERS measurements were performed by focusing the laser beam on the exposed face of a drop of suspended solution by using the plastic support described in the text (**Figure 3**) and for a maximum of 6 min time per drop. The support was subjected to a washing step with ethanol followed by plasma pre-treatment (Harrick Scientific Corp., PDC-002 operated at 60 Hz

and 0.2 Torr air) for 5 min before use. SERS data shown in **Figure 4 and Figure 7** represent an average as detailed in the caption; instead the spectra of **Figure 8** represent single acquisitions. The data at 638 nm are baseline corrected.

Characterization of particles and particle/protein interactions

The optical properties of the silver nanocubes were characterized by both a Jasco V-560 spectrophotometer and a bench spectrometer (EPP2000 by Stellarnet Inc.) connected to a Leica DM2500 microscope operated in transmission mode.

TEM and STEM analyses were performed in a (Cs)-probe-corrected JEOL ARM200CF at a primary beam energy of 200 keV operating in both transmission and scanning mode. The inner and outer collection angles of the annular dark-field detector were 68 and 280 mrad for annular dark field imaging. TEM samples were prepared by dropping a nanocube solution on a lacey-carbon TEM grid. STEM analysis was used for imaging the Ag nanocubes and its crystal lattice. With this technique in fact it is possible to image the position of the atomic column of Ag atoms along the e-beam direction. Due large differences in effective atomic number (Z) and thickness between Ag and the PVP, it was not possible to image both at the same time by using Z-contrast technique. To this purpose we used TEM bright field imaging. With this technique phase contrast helps to give much higher contrast between crystalline silver and amorphous PVP.

Methods used for FEM modeling as well as for MD simulations are described in Supporting Information.

ASSOCIATED CONTENT

Supporting Information Available. TEM analysis and TEM-based size distribution of silver nanocubes; extinction spectra of cytC and of Ag nanocubes; calculation of the number of cytC molecules per particle; procedure used for simulating the E-field distribution; extinction spectra before and after incubation with the protein; procedure used for MD simulations and additional results; SERS analysis, EF and G calculation for myoglobin. This material is available free of charge *via* the Internet at http://pubs.acs.org.

AUTHOR INFORMATION

Corresponding Author

*E-mail: p.matteini@ifc.cnr.it

Author Contributions

The manuscript was written through contributions of all authors. All authors have given approval to the final version of the manuscript. ‡These authors contributed equally.

ACKNOWLEDGMENT

P.M., M.C., M.A., and R.P. acknowledge the financial support from the Tuscany Region in the framework of PAR-FAS action line 1.1.2 SUPREMAL project. G.N. and M.S. acknowledge the Italian Ministry of Education and Research by the project Beyond-Nano (PON a3_00363). The work by E.P. and N.K. was supported by the Russian Scientific Foundation (project no. 14-13-01167).

TOC

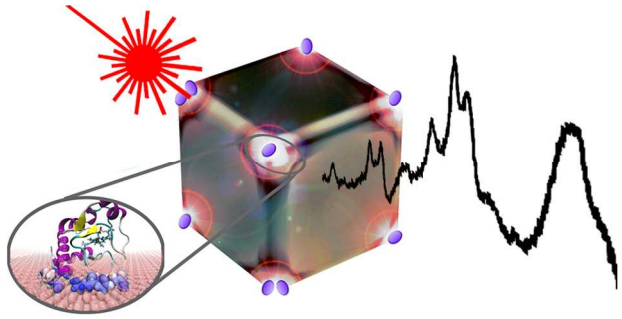

REFERENCES

(1) Le Ru, E. C.; Etchegoin, P. G. *Principles of Surface-Enhanced Raman Spectroscopy;* Elsevier: Oxford, 2009.
(2) Kneipp, K.; Moskovits, M.; Kneipp, H. *Surface-Enhanced Raman Scattering: Physics and Applications;* Springer-Verlag: Berlin Heidelberg, 2006.
(3) Willets, K. A.; Van Duyne, R. P. Localized Surface Plasmon Resonance Spectroscopy and Sensing. *Annu. Rev. Phys. Chem.* **2007,** *58*, 267-297.
(4) Prochazka, M. *Surface-Enhanced Raman Spectroscopy Bioanalytical, Biomolecular and Medical Applications*; Springer International Publishing: Switzerland, 2016.
(5) Kneipp, K.; Wang, Y.; Kneipp, H.; Perelman, L. T.; Itzkan, I.; Dasari, R.; Feld, M. S. Single Molecule Detection Using Surface-Enhanced Raman Scattering (SERS). *Phys. Rev. Lett.* **1997,** *78*, 1667-1670.
(6) Rodriguez-Lorenzo, L.; Alvarez-Puebla, R. A.; Pastoriza-Santos, I.; Mazzucco, S.; Stephan, O.; Kociak, M.; Liz-Marzan, L. M.; de Abajo, F. J. G. Zeptomol Detection through Controlled Ultrasensitive Surface-Enhanced Raman Scattering. *J. Am. Chem. Soc.* **2009,** *131*, 4616-4618.
(7) Podstawka , E.; Ozaki, Y. Surface-Enhanced Raman Difference between Bombesin and Its Modified Analogues on the Colloidal and Electrochemically Roughen Silver Surfaces. *Biopolymers* **2008,** *89*, 807-819.
(8) Ahijado-Guzman, R.; Gomez-Puertas, P.; Alvarez-Puebla, R. A.; Rivas, G.; Liz-Marzan, L. M. Surface-Enhanced Raman Scattering-Based Detection of the Interactions between the Essential Cell Division Ftsz Protein and Bacterial Membrane Elements. *ACS Nano* **2012,** *6*, 7514-7520.
(9) Kumar, G. V. P.; Reddy, B. A. A.; Arif, M.; Kundu, T. K.; Narayana, C. Surface-Enhanced Raman Scattering Studies of Human Transcriptional Coactivator P300. *J. Phys. Chem. B* **2006,** *110*, 16787-16792.

(10) Pazos, E.; Garcia-Algar, M.; Penas, C.; Nazarenus, M.; Torruella, A.; Pazos-Perez, N.; Guerrini, L.; Vazquez, M. E.; Garcia-Rico, E.; Mascarenas, J. L. *et al.* R. A. Surface-Enhanced Raman Scattering Surface Selection Rules for the Proteomic Liquid Biopsy in Real Samples: Efficient Detection of the Oncoprotein C-Myc. *J. Am. Chem. Soc.* **2016,** *138*, 14206-14209.
(11) Yang, S. K.; Dai, X. M.; Stogin, B. B.; Wong, T. S. Ultrasensitive Surface-Enhanced Raman Scattering Detection in Common Fluids. *Proc. Natl. Acad. Sci. U.S.A.* **2016,** *113*, 268-273.
(12) Banchelli, M.; Tiribilli, B.; de Angelis, M.; Pini, R.; Caminati, G.; Matteini, P. Controlled Veiling of Silver Nanocubes with Graphene Oxide for Improved Surface-Enhanced Raman Scattering Detection. *ACS Appl. Mater. Interfaces* **2016,** *8*, 2628-2634.
(13) Guerrini, L.; Arenal, R.; Mannini, B.; Chiti, F.; Pini, R.; Matteini, P.; Alvarez-Puebla, R. A. SERS Detection of Amyloid Oligomers on Metallorganic-Decorated Plasmonic Beads. *ACS Appl. Mater. Interfaces* **2015,** *7*, 9420-9428.
(14) Alvarez-Puebla, R. A.; Agarwal, A.; Manna, P.; Khanal, B. P.; Aldeanueva-Potel, P.; Carbo-Argibay, E.; Pazos-Perez, N.; Vigderman, L.; Zubarev, E. R.; Kotov, N. A. *et al.* Gold Nanorods 3d-Supercrystals as Surface Enhanced Raman Scattering Spectroscopy Substrates for the Rapid Detection of Scrambled Prions. *Proc. Natl. Acad. Sci. U.S.A.* **2011,** *108*, 8157-8161.
(15) Lee, P. C.; Meisel, D. Adsorption and Surface-Enhanced Raman of Dyes on Silver and Gold Sols. *J. Phys Chem.* **1982,** *86*, 3391-3395.
(16) Stockman, M. I. Nanoplasmonics: The Physics Behind the Applications. *Physics Today* **2011,** *64*, 39-44.
(17) Kurouski, D.; Sorci, M.; Postiglione, T.; Belfort, G.; Lednev, I. K. Detection and Structural Characterization of Insulin Prefibrilar Oligomers Using Surface Enhanced Raman Spectroscopy. *Biotechnol. Progr.* **2014,** *30*, 488-495.
(18) Macdonald, I. D. G.; Smith, W. E. Orientation of Cytochrome c Adsorbed on a Citrate-Reduced Silver Colloid Surface. *Langmuir* **1996,** *12*, 706-713.
(19) Dou, X. M.; Jung, Y. M.; Cao, Z. Q.; Ozaki, Y. Surface-Enhanced Raman Scattering of Biological Molecules on Metal Colloid II: Effects of Aggregation of Gold Colloid and Comparison of Effects of pH of Glycine Solutions between Gold and Silver Colloids. *Appl. Spectrosc.* **1999,** *53*, 1440-1447.
(20) Keating, C. D.; Kovaleski, K. K.; Natan, M. J. Heightened Electromagnetic Fields between Metal Nanoparticles: Surface Enhanced Raman Scattering from Metal-Cytochrome c-Metal Sandwiches. *J. Phys. Chem. B* **1998,** *102*, 9414-9425.
(21) Han, X. X.; Huang, G. G.; Zhao, B.; Ozaki, Y. Label-Free Highly Sensitive Detection of Proteins in Aqueous Solutions Using Surface-Enhanced Raman Scattering. *Anal. Chem.* **2009,** *81*, 3329-3333.
(22) Huang, G. G.; Han, X. X.; Hossain, M. K.; Ozaki, Y. Development of a Heat-Induced Surface-Enhanced Raman Scattering Sensing Method for Rapid Detection of Glutathione in Aqueous Solutions. *Anal. Chem.* **2009,** *81*, 5881-5888.
(23) Zhou, Z.; Huang, G. G.; Kato, T.; Ozaki, Y. Experimental Parameters for the SERS of Nitrate Ion for Label-Free Semi-Quantitative Detection of Proteins and Mechanism for Proteins to Form SERS Hot Sites: A SERS Study. *J. Raman Spectrosc.* **2011,** *42*, 1713-1721.
(24) Matteini, P.; de Angelis, M.; Ulivi, L.; Centi, S.; Pini, R. Concave Gold Nanocube Assemblies as Nanotraps for Surface-Enhanced Raman Scattering-Based Detection of Proteins. *Nanoscale* **2015,** *7*, 3474-3480.

(25) Ruan, W. D.; Ji, W.; Xue, X. X.; Cui, Y.; Chen, L.; Zhou, T. L.; Niu, L.; Li, X.; Zhang, J. H.; Zhao, B. SERS Detection of Proteins on Micropatterned Protein-Mediated Sandwich Substrates. *J. Raman Spectrosc.* **2011,** *42*, 1492-1496.
(26) David, C.; Guillot, N.; Shen, H.; Toury, T.; de la Chapelle, M. L. SERS Detection of Biomolecules Using Lithographed Nanoparticles Towards a Reproducible SERS Biosensor. *Nanotechnology* **2010,** *21*, 475501.
(27) De Luca, A. C.; Reader-Harris, P.; Mazilu, M.; Mariggio, S.; Corda, D.; Di Falco, A. Reproducible Surface-Enhanced Raman Quantification of Biomarkers in Multicomponent Mixtures. *ACS Nano* **2014,** *8*, 2575-2583.
(28) Fazio, B.; D'Andrea, C.; Foti, A.; Messina, E.; Irrera, A.; Donato, M. G.; Villari, V.; Micali, N.; Marago, O. M.; Gucciardi, P. G. SERS Detection of Biomolecules at Physiological pH Via Aggregation of Gold Nanorods Mediated by Optical Forces and Plasmonic Heating. *Sci. Rep.* **2016,** *6*, 26952.
(29) Skrabalak, S. E.; Au, L.; Li, X. D.; Xia, Y. N. Facile Synthesis of Ag Nanocubes and Au Nanocages. *Nature Protoc.* **2007,** *2*, 2182-2190.
(30) Panfilova, E. V.; Khlebtsov, B. N.; Burov, A. M.; Khlebtsov, N. G. Study of Polyol Synthesis Reaction Parameters Controlling High Yield of Silver Nanocubes. *Colloid J.* **2012,** *74*, 99-109.
(31) Al-Saidi, W. A.; Feng, H. J.; Fichthorn, K. A. Adsorption of Polyvinylpyrrolidone on Ag Surfaces: Insight into a Structure-Directing Agent. *Nano Lett.* **2012,** *12*, 997-1001.
(32) Xia, X. H.; Zeng, J.; Oetjen, L. K.; Li, Q. G.; Xia, Y. N. Quantitative Analysis of the Role Played by Poly(vinylpyrrolidone) in Seed-Mediated Growth of Ag Nanocrystals. *J. Am. Chem. Soc.* **2012,** *134*, 1793-1801.
(33) Rycenga, M.; Kim, M. H.; Camargo, P. H. C.; Cobley, C.; Li, Z. Y.; Xia, Y. N. Surface-Enhanced Raman Scattering: Comparison of Three Different Molecules on Single-Crystal Nanocubes and Nanospheres of Silver. *J. Phys. Chem. A* **2009,** *113*, 3932-3939.
(34) Lee, S. Y.; Hung, L.; Lang, G. S.; Cornett, J. E.; Mayergoyz, I. D.; Rabin, O. Dispersion in the SERS Enhancement with Silver Nanocube Dimers. *ACS Nano* **2010,** *4*, 5763-5772.
(35) Rycenga, M.; Xia, X. H.; Moran, C. H.; Zhou, F.; Qin, D.; Li, Z. Y.; Xia, Y. A. Generation of Hot Spots with Silver Nanocubes for Single-Molecule Detection by Surface-Enhanced Raman Scattering. *Angew. Chem. Int. Ed.* **2011,** *50*, 5473-5477.
(36) Spiro, T. G.; Strekas, T. C. Resonance Raman Spectra of Hemoglobin and Cytochrome c: Inverse Polarization and Vibronic Scattering. *Proc. Natl. Acad. Sci. U.S.A.* **1972,** *69*, 2622-2626.
(37) Cotton, T. M.; Schultz, S. S.; Van Duyne, R. P. Surface-Enhanced Resonance Raman Scattering from Cytochrome c and Myoglobin Adsorbed on a Silver Electrode. *J. Am. Chem. Soc.* **1980,** *102*, 7960-7962.
(38) Hildebrandt, P.; Stockburger, M. Surface-Enhanced Resonance Raman Spectroscopy of Cytochrome c at Room and Low Temperatures. *J. Phys. Chem.* **1986,** *90*, 6017-6024.
(39) Dick, L. A.; Haes, A. J.; Van Duyne, R. P. Distance and Orientation Dependence of Heterogeneous Electron Transfer: A Surface-Enhanced Resonance Raman Scattering Study of Cytochrome c Bound to Carboxylic Acid Terminated Alkanethiols Adsorbed on Silver Electrodes. *J. Phys. Chem. B* **2000,** *104*, 11752-11762.
(40) Delfino, I.; Bizzarri, A. R.; Cannistraro, S. Single-Molecule Detection of Yeast Cytochrome c by Surface-Enhanced Raman Spectroscopy. *Biophys. Chem.* **2005,** *113*, 41-51.

(41) Sivanesan, A.; Ly, H. K.; Kozuch, J.; Sezer, M.; Kuhlmann, U.; Fischera, A.; Weidinger, I. M. Functionalized Ag Nanoparticles with Tunable Optical Properties for Selective Protein Analysis. *Chem. Comm.* **2011,** *47*, 3553-3555.
(42) Filik, J.; Stone, N. Drop Coating Deposition Raman Spectroscopy of Protein Mixtures. *Analyst* **2007,** *132*, 544-550.
(43) Keating, C. D.; Kovaleski, K. M.; Natan, M. J. Protein : Colloid Conjugates for Surface Enhanced Raman Scattering: Stability and Control of Protein Orientation. *J. Phys. Chem. B* **1998,** *102*, 9404-9413.
(44) Niaura, G.; Gaigalas, A. K.; Vilker, V. L. Surface-Enhanced Raman Spectroscopy of Phosphate Anions: Adsorption on Silver, Gold, and Copper Electrodes. *J. Phys. Chem. B* **1997,** *101*, 9250-9262.
(45) Yeo, B. S.; Madler, S.; Schmid, T.; Zhang, W. H.; Zenobi, R. Tip-Enhanced Raman Spectroscopy Can See More: The Case of Cytochrome c. *J. Phys. Chem. C* **2008,** *112*, 4867-4873.
(46) Zhu, G. Y.; Zhu, X.; Fan, Q.; Wan, X. L. Raman Spectra of Amino Acids and Their Aqueous Solutions. *Spectrochim. Acta A Mol. Biomol. Spectrosc.* **2011,** *78*, 1187-1195.
(47) Fischer, W. B.; Eysel, H. H. Polarized Raman Spectra and Intensities of Aromatic Amino Acids Phenylalanine, Tyrosine and Tryptophan. *Spectrochim. Acta* **1992,** *48*, 725-732.
(48) Yu, Q.; Golden, G. Probing the Protein Orientation on Charged Self-Assembled Monolayers on Gold Nanohole Arrays by SERS. *Langmuir* **2007,** *23*, 8659-62.
(49) Peng, C. W.; Liu, J.; Zhou, J. Molecular Simulations of Cytochrome c Adsorption on a Bare Gold Surface: Insights for the Hindrance of Electron Transfer. *J. Phys. Chem. C* **2015,** *119*, 20773-20781.
(50) Zhou, Y. X.; Nagaoka, T.; Zhu, G. Y. Electrochemical Studies of Cytochrome c Disulfide at Gold Electrodes. *Biophys. Chem.* **1999,** *79*, 55-62.
(51) Smulevich, G.; Spiro, T. G. Surface Enhanced Raman Spectroscopic Evidence That Adsorption on Sllver Particles Can Denature Heme Proteins. *J. Phys. Chem.* **1985,** *89*, 5168-5173.
(52) Treuel, L.; Malissek, M.; Grass, S.; Diendorf, J.; Mahl, D.; Meyer-Zaika, W.; Epple, M. Quantifying the Influence of Polymer Coatings on the Serum Albumin Corona Formation around Silver and Gold Nanoparticles. *J. Nanopart. Res.* **2012,** *14*, 1102.
(53) Podila, R.; Chen, R.; Ke, P. C.; Brown, J. M.; Rao, A. M. Effects of Surface Functional Groups on the Formation of Nanoparticle-Protein Corona. *Appl. Phys. Lett.* **2012,** *101*.
(54) Chen, T.; Du, C. L.; Tan, L. H.; Shen, Z. X.; Chen, H. Y. Site-Selective Localization of Analytes on Gold Nanorod Surface for Investigating Field Enhancement Distribution in Surface-Enhanced Raman Scattering. *Nanoscale* **2011,** *3*, 1575-1581.
(55) Millstone, J. E.; Georganopoulou, D. G.; Xu, X. Y.; Wei, W.; Li, S. Y.; Mirkin, C. A. DNA-Gold Triangular Nanoprism Conjugates. *Small* **2008,** *4*, 2176-2180.
(56) Le Ru, E. C.; Blackie, E.; Meyer, M.; Etchegoin, P. G. Surface Enhanced Raman Scattering Enhancement Factors: A Comprehensive Study. *J. Phys. Chem. C* **2007,** *111*, 13794-13803.
(57) Khlebtsov, B. N.; Khanadeev, V. A.; Panfilova, E. V.; Bratashov, D. N.; Khlebtsov, N. G. Gold Nanoisland Films as Reproducible SERS Substrates for Highly Sensitive Detection of Fungicides. *ACS Appl. Mater. Interfaces* **2015,** *7*, 6518-6529.
(58) Zito, G.; Rusciano, G.; Pesce, G.; Dochshanov, A.; Sasso, A. Surface-Enhanced Raman Imaging of Cell Membrane by a Highly Homogeneous and Isotropic Silver Nanostructure. *Nanoscale* **2015,** *7*, 8593-8606.

(59) Similar conclusions have be been obtained on other proteins: see the case of myoglobin in Supporting Information
(60) Xu, L. J.; Zong, C.; Zheng, X. S.; Hu, P.; Feng, J. M.; Ren, B. Label-Free Detection of Native Proteins by Surface-Enhanced Raman Spectroscopy Using Iodide-Modified Nanoparticles. *Anal. Chem.* **2014,** *86*, 2238-2245.
(61) Kahraman, M.; Balz, B. N.; Wachsmann-Hogiu, S. Hydrophobicity-Driven Self-Assembly of Protein and Silver Nanoparticles for Protein Detection Using Surface-Enhanced Raman Scattering. *Analyst* **2013,** *138*, 2906-2913.
(62) Zhou, Z.; Han, X. X.; Huang, G. G.; Ozaki, Y. Label-Free Detection of Binary Mixtures of Proteins Using Surface-Enhanced Raman Scattering. *J. Raman Spectrosc.* **2012,** *43*, 706-711.
(63) Rabe, M.; Verdes, D.; Seeger, S. Understanding Protein Adsorption Phenomena at Solid Surfaces. *Adv. Colloid Interface Sci.* **2011,** *162*, 87-106.
(64) Que, R. H.; Shao, M. W.; Zhuo, S. J.; Wen, C. Y.; Wang, S. D.; Lee, S. T. Highly Reproducible Surface-Enhanced Raman Scattering on a Capillarity-Assisted Gold Nanoparticle Assembly. *Adv. Funct. Mater.* **2011,** *21*, 3337-3343.